Raman Spectroscopic Measurement of Oxidation in Supercritical Water. 1. Conversion of Methanol to Formaldehyde

Steven F. Rice,* Thomas B. Hunter, Åsa C. Rydén,† and Russell G. Hanush

Combustion Research Facility, Sandia National Laboratories, P.O. Box 969, Livermore, California 94551-0969

The oxidation rate of methanol and the subsequent production and destruction of the primary intermediate, formaldehyde, were investigated using Raman spectroscopy as an *in situ* analytical method. Experiments were conducted in supercritical water over temperatures ranging from 440 to 500 °C at 24.1 MPa and at a nominal feed concentration of 0.05 mol/L (1.5 wt %). Effluent samples were also examined using gas chromatography. In these experiments, feed concentrations ranging from 0.011 to 1.2 wt % and temperatures from 430 to 500 °C were examined and showed that the effective first-order reaction rate for the oxidation of methanol is dependent on the initial feed concentration. Raman measurements reveal a temperature-dependent induction period of less than 1 s over the range of conditions investigated. In addition, quantitative measurements of the production of formaldehyde indicate it is a key metastable intermediate. An elementary reaction mechanism, which reproduces accurately the quantitative features of methanol oxidation and formaldehyde production, is used to identify key rate controlling reactions during the induction period and the transition to the primary oxidation path.

Introduction

Industrial oxidation processes for chemical manufacturing and combustion processes for power generation have historically operated in two different reaction regimes. Industrial oxidation requires mild pressures and temperatures in the 100–300 °C range and typically is conducted with the assistance of a catalyst. Both gas phase and liquid phase operation are common. Combustion is considered a gas phase process and is generally conducted at pressures ranging from ambient to tens of atmospheres and temperatures above 1000 °C. Recently, interest in chemical processing in supercritical fluids has placed emphasis on understanding the relationships between high-temperature, low-density combustion processes and intermediate-temperature oxidation at near-liquid-like densities. An example of this reaction regime, which has characteristics falling between combustion and most conventional chemical processing, is hydrothermal processing; supercritical water oxidation (SCWO) can be considered a special application in this regime.

Hydrothermal oxidation processes, including supercritical water oxidation, are emerging as effective methods for the destruction of hazardous and nonhazardous industrial aqueous wastes (Barner *et al.*, 1992; Modell, 1985; Swallow *et al.*, 1989). The SCWO process is conducted at temperatures and pressures (typically 450–650 °C and 24 MPa) above the critical point of water (374 °C and 22.1 MPa) and is considered applicable to aqueous waste streams containing 0–20% organics (Tester *et al.*, 1991).

As this technology has become commercially available (Gloyna *et al.*, 1994; McBrayer, 1995), interest in process development research has been shifting from feasibility demonstration to the evaluation of process scale-up costs. In order to accurately evaluate these costs, operational reaction condition tradeoffs with regard to pressure, temperature, and reaction duration need to be considered. This evaluation will be hindered without better predictive models for the time, temperature, density, and concentration dependence of organic oxidation rates at hydrothermal conditions.

The current understanding of reaction kinetics in supercritical water is limited to a handful of global rate expressions for simple chemicals (Li *et al.*, 1991; Tester *et al.*, 1991). These expressions serve to bracket potential operating parameters for particular species, but are of limited use in the formulation of predictive models for SCWO equipment design. To be generally applicable and valuable as a design tool, models should be based on elementary reaction steps, or at least on a mechanistic description that incorporates all of the key fundamental reactions.

Much of the experimental work to date on reaction kinetics in supercritical water has used sample-and-quench techniques followed by chromatographic analysis to develop reaction time–temperature kinetic relationships. These techniques have produced global expressions for fuel consumption and in some instances have been used to develop quantitative reaction pathway descriptions based on elementary reaction mechanisms (Holgate and Tester, 1994a,b). However, agreement between elementary models and experiment is only qualitative in most cases (Helling and Tester, 1987; Webley and Tester, 1989, 1991).

Recently, optical diagnostics have been employed to detect solutes in supercritical water using windowed reaction vessels to determine chemical equilibrium, decomposition reactions, and bulk phenomena (Armellini and Tester, 1991, 1993; Masten *et al.*, 1993; Shaw *et al.*, 1991; Spohn and Brill, 1989; Steeper *et al.*, 1992). Previously, Raman spectroscopy has proven to be a useful method for measuring concentrations of a variety of chemical species in supercritical water in a constant volume reactor. Signals have been recorded for CH_4, CH_3OH, CO_2, CO, H_2, O_2, and N_2 at concentrations well below 0.01 mol/L (Steeper *et al.*, 1996). We have extended this experimental approach, using Raman spectroscopy in a high-pressure flow reactor, permitting examination of species concentration profiles in supercritical water for feeds of two or more reactants as a function of time and temperature. This work demon-

* Corresponding author (sfrice@sandia.gov).

† Present address: Department of Chemical Engineering II, Chemical Center, Lund University, P.O. Box 124, S-221 00 Lund, Sweden.

S0888-5885(95)00510-0 CCC: $12.00

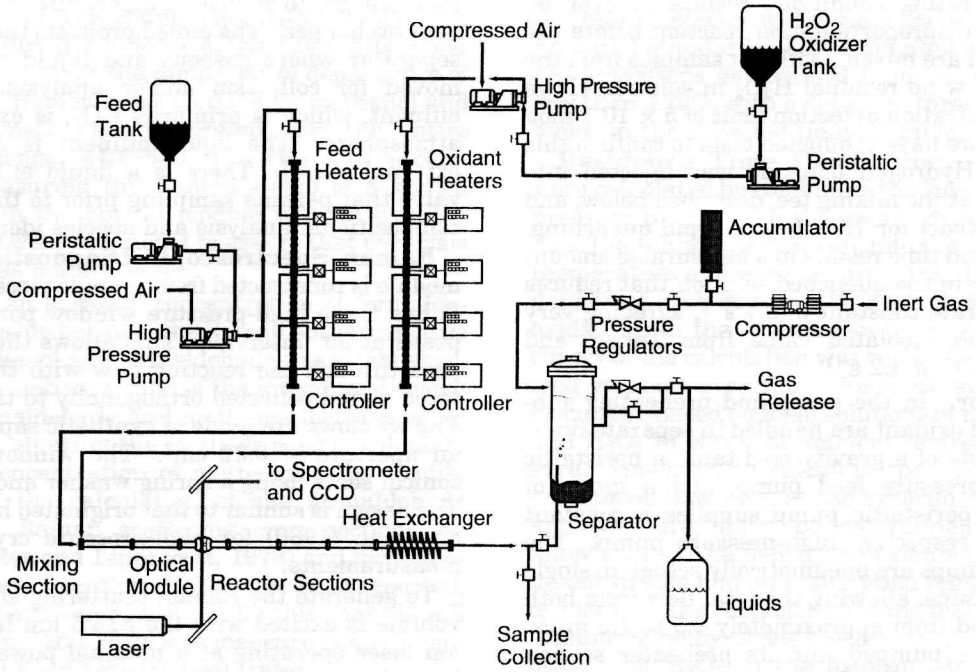

Figure 1. Schematic of the Sandia supercritical water oxidation flow reactor.

strates the power of optical methods for collecting the detailed experimental data necessary to describe chemical reactivity over a wide range of pressures, temperatures, and reactant feed concentrations.

Methanol was chosen as the initial species to investigate because of its presumed simple oxidation chemistry. Accurate high-temperature models are available with which to compare hydrothermal results, along with well documented experimental measurements at lower pressures (Norton and Dryer, 1989, 1990). In addition, methanol is likely to have only a small set of intermediates, many of which should be observable.

We have examined methanol oxidation using two methods. The primary technique was to examine the disappearance of methanol and the formation of formaldehyde using Raman spectroscopy. In addition, sample-and-quench methods followed by gas chromatographic analysis were used to measure the methanol oxidation rate over a concentration range extending from practical waste feed concentrations down to concentrations typical of past SCWO studies.

We report here the results from a series of experiments examining the oxidation of methanol by oxygen at 440–500 °C and 24.1 MPa. These experimental results are compared to the predictions from several recently developed elementary reaction models identifying one model in particular that reproduces the experimental results well. The data are analyzed in a variety of ways and compared to general characteristics of the successful model. The analysis of the model is used to identify key reactions in this experimental temperature and density regime and to illuminate the critical role that the stability of H_2O_2 plays in determining the overall oxidation rate.

This paper reports experimental kinetic measurements using a new technique with interpretation of the results presented in the context of elementary reaction modeling. It presents an experimental confirmation of a model developed by other researchers (Schmitt *et al.*, 1991). Results from interpretation of a sensitivity analysis of this model are reported here; however, the successful elementary model was not developed in this work, and therefore is not presented in detail.

Experimental Section

All of the oxidation experiments presented were conducted in a high-pressure, optically-accessible flow reactor capable of continuous operation at temperatures up to 620 °C and pressures of 45.0 MPa. In the following section, the experimental systems and procedures are discussed briefly; however, additional detail, including reactor control and acquisition of pressure and temperature data, can be found elsewhere (Hanush *et al.*, 1995). The optically-accessible flow reactor, see Figure 1, consists of three major subsystems: pump and preheating, reactor, and cooling and separation. Each subsystem is described below accompanied by brief descriptions of the optical module and the Raman spectroscopic system.

Reactants. For all Raman spectroscopic experiments the oxidant was O_2, supplied as a solution of hydrogen peroxide (H_2O_2) in the oxidant preheater. The H_2O_2 feeds were 5.5, 2.75, and 1.37 wt % in water. The decomposition of H_2O_2 to O_2 during preheat is discussed below. The fuel feed was 1.5 wt % methanol in a balance of water. Each feed was prepared by adding the appropriate mass of water (McKesson Water Products Co., deionized) to either pure methanol (Aldrich, spectrophotometric grade) or 30 wt % H_2O_2 (J. T. Baker, electronic grade). All reactants were used as received.

The oxidizer is fed to the system in the form of a solution of H_2O_2 that is subsequently thermally decomposed in the preheating section to a high-pressure mixture of O_2 in supercritical water. It is critical that the H_2O_2 be completely converted to O_2 to assure the reliability of the experimental results. The conversion rate has been estimated based on the results obtained by Takagi and Ishigure (1985). They found that the decomposition of H_2O_2 in liquid-density water for temperatures up to 280 °C has an Arrhenius behavior with a first-order rate constant of 0.24 s^{-1} at 280 °C. Extrapolating this experimental temperature dependence to 450 °C yields a rate constant of 9.4 s^{-1}. Using the maximum oxidizer flow rate for our experiments, about 0.8 g/s, the residence time in the preheating subsystem is approximately 7 s at 450 °C. This com-

bination of operating conditions results in over 60 lifetimes of the disproportionation reaction before the oxidizer and fuel are mixed. Effluent samples from the oxidizer line show no residual H_2O_2 in solution above our iodometric titration detection limit of 5×10^{-5} mol/L. In addition, we have conducted tests to confirm this extrapolation. Hydrogen peroxide was injected into water at 390 °C at the mixing tee, described below, and permitted it to react for 1.7 s before rapid quenching. This short reaction time results in a measurable amount of residual H_2O_2 in the quenched solution that reduces to a first-order rate constant of 3.1 s^{-1}, agreeing very well with the extrapolated value from Takagi and Ishigure at 390 °C of 3.2 s^{-1}.

Flow Reactor. In the pump and preheating subsystem, fuel and oxidant are handled in separate lines. Each line consists of a gravity feed tank, a peristaltic pump, a high-pressure feed pump, and a group of heaters. Each peristaltic pump supplies a constant pressure to its respective high-pressure pump. The high-pressure pumps are pneumatically actuated, single stage, piston pumps, allowing the total flow from both lines to be varied from approximately 0.5 to 1.6 mL/s. Each reactant is pumped into its preheater section consisting of a length of high-pressure tubing contained in four 875 W radiant tube furnaces and a section wrapped with two 375 W cable heaters. All of the preheater high−pressure tubing is Inconel 625, 0.48 cm (3/16 in.) inner diameter (i.d.) and 1.43 cm (9/16 in.) outer diameter (o.d.). The total length of the preheater is 310 cm. The sections are joined with Autoclave Engineers Inconel 625 high-pressure unions. A 1/16 in., Inconel sheathed, Type K thermocouple is installed in each union to measure the fluid temperature and provide feedback to the appropriate heater controller. Thermocouples are also installed on all tubing surfaces to monitor for overheating. All exposed heated sections and unions are wrapped with alumina insulation to minimize heat loss.

The heated fuel and oxidant streams, at the desired experimental temperature, are mixed under turbulent conditions by combining the flows at a 180° angle of incidence. The combined flow exits the mixing tee orthogonally to the original flows. For the current work, Reynolds numbers of the combined flow range from 4800 to 14 700, ensuring turbulent flow in the reactor over the entire operating range.

The combined flows then pass into the reactor subsystem. The reactor consists of six 61-cm sections of Inconel 625 tubing (0.48 cm i.d. and 1.43 cm o.d.) joined by Autoclave Engineers Tee fittings with Type K thermocouples inserted into the centerline of the flow. These thermocouples measure the fluid temperatures and provide feedback for the reactor temperature controllers. The optical module, used for Raman measurements, can be installed at any point along the entire 380 cm length of the reactor. This allows a range of residence times, from approximately 0.1 to 83 s, to be examined. Each of the reactor sections is wrapped with a 375 W cable heater and is insulated to minimize heat loss and allow isothermal operation of the flow reactor. In addition, each length of tubing can be wrapped with air cooling coils for the removal of heat from the reaction if needed.

The cooling and separation subsystem consists of a convective heat exchanger, a water-cooled, counter-flow heat exchanger, and a gravity separator. The reacting flow is first cooled in the convective heat exchanger and then brought to ambient temperature in the counterflow heat exchanger. The cooled products then pass into the separator where gaseous and liquid effluent are removed for collection and/or analysis. The gaseous effluent, which is primarily CO_2, is exhausted to the atmosphere. The liquid effluent is collected in an external vessel. There is a liquid effluent sampling valve that permits sampling prior to the separator for compositional analysis and species identification.

Raman Spectroscopic Diagnostic. The optical module is constructed from a single piece of Inconel 625. It has three high-pressure window ports, radially opposed at 90° intervals. This allows the laser beam to pass through the reacting flow with the Raman-scattered signal collected orthogonally to the pump beam. The windows are made of synthetic sapphire and have an aperture of 0.32 cm^2. The windows are held in conical seats using a spring washer and nut assembly. The design is similar to that originated by Abdullah and Sherman (1980) for high-pressure cryogenic Raman measurements.

To generate the Raman scattering signal, the probe volume is excited with the 514.5 nm line of an argon ion laser operating at a nominal power of 2 W. The beam is focused into the optical module with a 500 mm focal length lens producing a pump beam diameter of approximately 0.06 mm. The scattered light is collected with an f/3 aperture and imaged through a lens and mirror system onto the entrance slit of a 0.5-m single spectrometer, equipped with a 2400 rule/mm grating. To aid in rejection of the scattered laser light, a colored glass filter (RG 570) is employed in front of the spectrometer. The relevant portion of the Raman spectrum is imaged onto a 384 × 576 pixel CCD array. The resulting Raman signal is collected, processed, and stored using an in-house data acquisition program (Hanush *et al.*, 1995).

Concentration Measurement. The power of the Raman signal, P_r, can be expressed as

$$P_r = P_i n(\partial\sigma/\partial\Omega)\Omega l\epsilon \qquad (1)$$

where P_i is the pump laser power, n is the species number density, $\partial\sigma/\partial\Omega$ is the differential Raman cross section, Ω is the collection solid angle, l is the sampling extent, and ϵ is the collection efficiency (Eckbreth, 1988). It is evident that the Raman signal power is directly proportional to the species number density. Therefore, by integrating the observed intensity of a Raman band over wavelength, a value which is proportional to the species concentration can be obtained. Therefore, the absolute concentration of a species can be calculated following calibration of the system. Methanol concentrations were quantified using the integrated intensity of the lower energy C−H stretch of methanol centered at a Raman shift of 2843 cm^{-1}; formaldehyde concentrations were determined using the C−H stretch centered at a Raman shift of 2780 cm^{-1} (Grasselli and Bulkin, 1991; Sadtler, 1973).

The optical system was calibrated by flowing a known concentration of methanol, without oxidizer, through the optical module and recording the resulting Raman signal. To account for changes in the parameters of eq 1 which could affect the absolute magnitude of the signal over time, each species signal was ratioed to the O−H stretch from water, centered at a Raman shift of ~3628 cm^{-1}. By normalizing the species signal to the water signal, any drift in the system parameters in eq

1 (notably, P_i and ϵ) is accounted for, with the exception of the temperature dependence of the differential cross section. To account for the temperature dependence of the differential Raman cross sections for methanol and water, the signals were calibrated over the entire temperature range, 440−500 °C. This was accomplished by measuring the Raman signal of a known concentration in the optical module without oxidizer present. Tests were conducted to assure that pyrolysis of methanol was not an issue.

To measure an absolute concentration of formaldehyde, a relationship between the Raman scattering cross sections of methanol and formaldehyde was established. Given this information, a ratio of the integrated intensities of the formaldehyde and methanol features could be determined, allowing the methods used to calculate the absolute concentration of methanol to be readily transferred to the calculation of the formaldehyde concentration. Raman scattering cross sections for methanol (Nestor and Lippincott, 1973) and formaldehyde (Surkin and Sverdlov, 1980) have been reported; however, the relative cross sections for this analysis will be more reliable if this ratio was measured experimentally above 400 °C in supercritical water.

To establish this ratio, the spectrum of a known mixture at conditions near those in our oxidation measurements was recorded. Using a cell reactor (Steeper, 1995), a solution of 3.12 mol/L formaldehyde and 2.74 mol/L methanol was injected into a preheated reactor filled with supercritical water at 408 °C and 24.1 MPa. Immediately following injection, the 2800 cm^{-1} region of the Raman spectrum, covering both the methanol and formaldehyde features, was recorded at 1-s intervals. Total injection time was about 3 s. After less than a minute, the formaldehyde signal began to decrease significantly, most likely the result of a hydrolysis or polymerization reaction. However, a reproducible peak intensity ratio was recorded for the first 15 scans. A value of 1.37 was determined for the ratio of the formaldehyde cross section to that of methanol and was used for the determination of the concentration of formaldehyde.

Concentrations are calculated by integrating the area under the Raman peak and applying the appropriate calibration. When two slightly overlapping peaks are present, as is the case with methanol and formaldehyde, an approximation must be made to perform the integration. In this case, the area of each peak is calculated by integrating from the tail of the peak to the minimum point of their overlapping region. Since the amount of overlap between the methanol and formaldehyde peaks is small, the error in this approximation is insignificant relative to the noise on the data. The uncertainty in determining the concentration from the integration of a single peak, based solely on a statistical analysis of the noise associated with the measurement technique, is less than ±2.5% (95% confidence) of full scale. This sets the minimum detection limit at about 1/20 of the feed concentration 1.5 wt % methanol (2.3×10^{-3} mol/L at typical experimental conditions).

Gas chromatography (GC) was used to quantify the effluent species concentration for several experimental conditions. Samples were obtained prior to the separator using a sampling valve, and residence times were calculated, as discussed below, with the additional assumption that the reaction was quenched promptly, estimated to be 0.3 s, after entering the cooling subsystem. Concentrations were determined using a flame ionization detector whose response was calibrated with prepared standards. The estimated uncertainty in the concentrations determined from GC measurements is less than ±10%, with a detection threshold of 2.9×10^{-4} mol/L in the collected liquid sample.

Residence Time Calculation. Residence times were calculated by combining the frequency of the high-pressure pumps with the known displacement, to produce the volumetric flow rate into the system at ambient temperature and elevated pressure. By calculating the density of each stream, the mass flow rate of fuel and oxidizer into the system can be determined. The accuracy of the calculation was verified by measuring total feed volumes over time. Feed stream densities were calculated based on ideal solutions of methanol in water and H_2O_2 in water at ambient temperature and pressure. However, to calculate the residence time, the volumetric flow rate, at the experimental temperature and pressure, must be determined. This requires knowledge of the density and composition of the final mixed stream and an assumption regarding the mixing of species. The composition of the fuel stream is known (assuming no pyrolysis has occurred). As stated previously, the H_2O_2 in the oxidizer stream rapidly and completely undergoes decomposition to form O_2 and H_2O when heated to the reaction temperature; therefore, the composition of the oxidizer stream can also be determined.

Lastly, an accurate equation of state is needed for the mixture of water, fuel, and oxygen. If it is assumed that the species mix to form an ideal solution, the density of each pure component is all that is necessary to complete the calculation. The density of water at reaction conditions is calculated using NBS Steam Tables (Haar *et al.*, 1984). The density of fuel, which accounts for only 0.8 mol % of the final mixture, was assumed equal to that of water. Finally, the density of O_2 was calculated at experimental conditions using a generalized compressibility factor correction to the ideal gas law (O_2 accounts for approximately 1.5 mol % of the final mixture, for most runs). With the density and the mass flow rate, the residence time (from the mixing point) can be calculated by making a plug flow approximation. All reported residence times were calculated in this manner and represent the time from the mixing point to the Raman measurement point or the quenching location.

Within these approximations, the calculation of residence time is directly proportional to density at all flow rates. The possible deviation in actual density at these low concentrations of fuel and oxidizer streams relative to this theoretical calculation using the empirical equation of state of water and ideal mixing will be on the order of several percent and not grossly affect the validity of the results.

Results

Table 1 shows the results of 19 GC measurements of the oxidation of methanol in supercritical water over the temperature range of 430−500 °C and initial feed concentrations ranging from 0.011 to 1.2 wt %. All experiments were conducted at a fuel-to-oxidizer equivalence ratio of 0.66. The residence time of each sample was 7.0 s at reaction temperature and 27.4 MPa.

An Arrhenius plot for the GC results is shown in Figure 2. In the figure, the observed normalized methanol concentration, $[CH_3OH]/[CH_3OH]_0$, is related

Table 1. Oxidation of Methanol at Varying Initial Concentrations (Based on GC Analysis)

temp (°C)	$[CH_3OH]_0$ (wt %)[a]	$[CH_3OH]/[CH_3OH]_0$[a]	k_{eff}[b] (s^{-1})
430	0.011	0.95	0.0073
450	0.011	0.86	0.0022
460	0.011	0.85	0.0023
470	0.011	0.069	0.38
480	0.011	0.0029	0.50
440	0.056	0.83	0.027
460	0.056	0.79	0.034
480	0.056	0.082	0.36
500	0.056	0.018	0.58
430	0.39	0.27	0.019
440	0.39	0.12	0.30
450	0.39	0.016	0.59
450	0.39	0.0082	0.36
460	0.39	0.0051	0.75
480	0.39	0.0056	0.076
440	1.2	0.088	0.35
450	1.2	0.021	0.55
460	1.2	0.0021	0.88
470	1.2	0.0015	0.93

[a] $[CH_3OH]_0$ is the initial methanol concentration. [b] k_{eff} is the effective first-order rate constant.

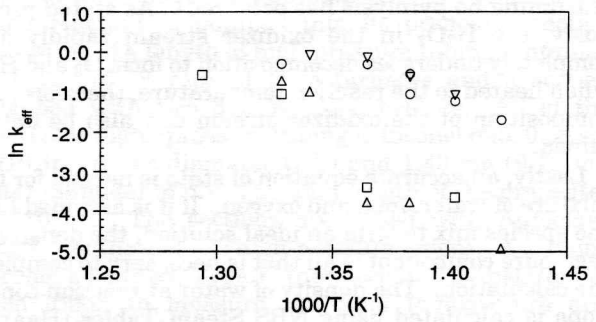

Figure 2. Arrhenius plot of the effective first-order rate constant, k_{eff}, versus $1000/T$ for various initial CH_3OH feed concentrations: 0.011 wt % △, 0.056 wt % □, 0.39 wt % ○, 1.2 wt % ▽. All results are from the sample-and-quench technique and subsequent analysis by gas chromatography.

to an effective first-order rate constant, k_{eff}, defined by

$$k_{eff} = -\ln\left(\frac{[CH_3OH]}{[CH_3OH]_0}\right)(t)^{-1} \qquad (2)$$

where $[CH_3OH]_0$ is the initial methanol concentration, $[CH_3OH]$ is the measured effluent concentration, and t is the residence time. It is evident that the effective first-order rate constant varies significantly with initial feed concentration. Higher initial feed concentrations exhibit greater effective reaction rate constants than low feed concentrations. In addition, the conversion rate for the low feed concentrations appears to increase more steeply with temperature. Other than the empirical utility of the conversion-versus-residence time data, there is an important observation to be drawn from this experiment. Since all of the data points do not fall on the same line, the results show that a first-order representation of the data is not a good description of the rate behavior over a wide range of feed concentration. This implies, given a high initial feed concentration, that the same effective rate that describes the oxidation of rate for the first 90% of conversion of an industrial feed may not accurately describe the conversion from 99.9% to 99.99%. The data also show that the same effective activation energy for the reaction, represented by the slope of the plot for a given feed concentration as a function of temperature, varies with the initial feed. At high fuel concentration, the activation energy is distinctly less than at low fuel feeds. This suggests that the rate limiting step or steps consuming the bulk of the initial methanol at high concentration are not the same when the fuel concentration is low.

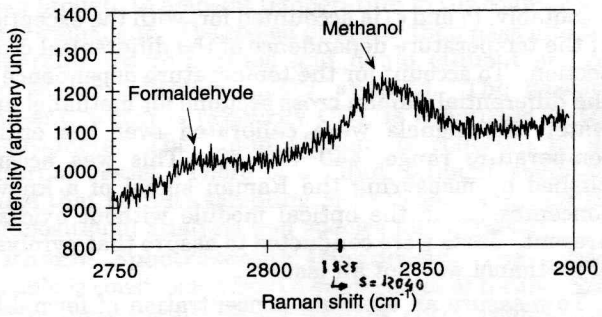

Figure 3. Raman spectrum of the reacting mixture of methanol and formaldehyde for initial conditions of 500 °C, 5.5 wt % H_2O_2, 1.5 wt % CH_3OH (equivalence ratio 0.85), and a pressure 24.1 MPa.

Figure 3 shows a typical spectrum of the 2837 cm^{-1} C−H stretching vibrational feature of methanol and the 2775 cm^{-1} C−H stretching resonance of formaldehyde in supercritical water at 500 °C and 24.1 MPa. In the gas phase, the methanol band appears at 2843 cm^{-1} and the formaldehyde band appears at 2780 cm^{-1}. Although the conditions in the supercritical fluid are probably best described as a dense gas, spectroscopically, the Raman band exhibits no rotational structure, even when recorded at much higher resolution.

Raman spectra were recorded during methanol oxidation in the flow reactor at 24.1 MPa for 196 different combinations of optical module position, flow rate, equivalence ratio, and temperature. All of the data points were collected at an ambient methanol feed concentration of 0.47 mol/L, which corresponds to a fuel concentration ranging from 0.051 mol/L at 440 °C and 24.1 MPa to 0.041 mol/L at 500 °C and 24.1 MPa. Most experiments were conducted at an H_2O_2 concentration of 1.65 mol/L corresponding to a fuel-to-oxidizer equivalence ratio of 0.85. However, additional experiments were performed at equivalence ratios of 1.65 and 3.40 by adjusting the initial H_2O_2 concentration accordingly. Therefore, reaction conditions from fuel lean to fuel rich were tested.

Table 2 presents the results from 114 measurements at an equivalence ratio of 0.85. The data were obtained with the optical module located at three different positions within the reactor, specifically, 17.8, 45.7, and 81.2 cm. For each position of the optical module, the flow velocity generally was varied from 30 to 105 cm/s. As a result, there is significant overlap in residence times for the three optical module positions, allowing the reproducibility of the data to be verified.

Previously, it was determined, based on extrapolation of lower temperature results, that H_2O_2 is completely converted to O_2 in the preheating section. The current experimental results presented in Table 2 support this conclusion. Close inspection indicates that the three optical module locations produce results that smoothly overlap. To create the same residence time given two different optical module locations requires that the flow rate be properly adjusted. For example, if the module is located at position 1, i.e., close to the mixing point, the flow rate must be decreased relative to the flow rate necessary for production of an equal residence time with the module at position 2. When the module is at position 2 with an increased flow rate, the oxidizer

Table 2. Methanol and Formaldehyde Detected by Raman Spectroscopy

temp (°C)	t^a (s)	cell position[b]	$[CH_3OH]/[CH_3OH]_0$[c]	$[CH_2O]/[CH_3OH]_0$[c]	temp (°C)	t^a (s)	cell position[b]	$[CH_3OH]/[CH_3OH]_0$[c]	$[CH_2O]/[CH_3OH]_0$[c]
440	0.231	1	1.04	0.001	470	0.487	1	0.87	0.082
440	0.536	2	0.94	0.005	470	0.506	1	0.88	0.112
440	0.580	1	1.03	0.001	470	0.508	1	0.80	0.067
440	0.746	2	0.96	0.035	470	0.553	1	0.79	0.107
440	0.772	1	0.98	0.001	470	0.601	1	0.75	0.126
440	1.012	2	0.90	0.067	470	0.649	2	0.77	0.128
440	1.191	2	0.82	0.090	470	0.672	1	0.81	0.080
440	1.347	2	0.77	0.099	470	0.711	1	0.75	0.126
440	1.494	2	0.73	0.131	470	0.741	1	0.74	0.135
440	1.682	2	0.69	0.128	470	0.842	1	0.64	0.141
450	0.220	1	1.04	0.004	470	0.854	2	0.62	0.139
450	0.505	2	0.96	0.043	470	1.071	2	0.28	0.078
450	0.552	1	1.00	0.000	470	1.196	2	0.20	0.075
450	0.709	2	0.86	0.062	470	1.298	2	0.00	0.000
450	0.735	1	0.92	0.032	470	1.418	2	0.00	0.000
450	0.918	2	0.82	0.110	480	0.176	1	1.03	0.049
450	0.938	3	0.82	0.095	480	0.250	1	0.90	0.076
450	1.201	2	0.74	0.108	480	0.312	1	0.82	0.108
450	1.276	3	0.77	0.127	480	0.388	1	0.71	0.145
450	1.278	2	0.65	0.129	480	0.448	1	0.79	0.136
450	1.424	2	0.63	0.128	480	0.553	1	0.61	0.111
450	1.619	2	0.54	0.132	480	0.605	1	0.55	0.146
450	1.884	3	0.54	0.119	480	0.648	1	0.42	0.113
450	2.125	3	0.58	0.119	480	0.772	1	0.27	0.106
450	2.282	3	0.35	0.071	480	0.839	2	0.34	0.122
450	2.463	3	0.32	0.062	480	0.849	1	0.39	0.115
450	2.747	3	0.35	0.059	480	1.044	2	0.00	0.000
450	2.876	3	0.28	0.066	480	1.139	2	0.00	0.000
460	0.210	1	1.00	0.004	480	1.263	2	0.00	0.000
460	0.492	2	0.86	0.072	480	1.371	2	0.00	0.000
460	0.497	1	0.75	0.056	490	0.170	1	0.88	0.067
460	0.527	1	0.96	0.000	490	0.172	1	0.93	0.000
460	0.561	1	0.81	0.052	490	0.242	1	0.83	0.106
460	0.632	1	0.78	0.087	490	0.244	1	0.87	0.108
460	0.680	2	0.83	0.124	490	0.309	1	0.79	0.121
460	0.697	1	0.88	0.059	490	0.311	1	0.72	0.145
460	0.750	1	0.74	0.080	490	0.376	1	0.75	0.174
460	0.810	1	0.68	0.112	490	0.381	1	0.59	0.191
460	0.849	1	0.76	0.085	490	0.438	1	0.59	0.140
460	0.879	2	0.63	0.126	490	0.455	1	0.50	0.154
460	0.896	3	0.77	0.150	490	0.513	1	0.48	0.160
460	0.983	1	0.55	0.044	490	0.519	1	0.42	0.091
460	1.132	2	0.47	0.125	490	0.581	1	0.33	0.084
460	1.177	3	0.57	0.121	490	0.594	1	0.23	0.086
460	1.235	2	0.50	0.131	490	0.619	1	0.43	0.105
460	1.363	2	0.39	0.113	490	0.645	1	0.37	0.094
460	1.457	2	0.20	0.074	490	0.732	1	0.26	0.074
460	1.616	3	0.29	0.055	490	0.733	1	0.28	0.068
460	2.006	3	0.20	0.013	490	0.773	1	0.17	0.115
460	2.028	3	0.23	0.045	490	0.796	1	0.15	0.028
460	2.671	3	0.07	0.000	500	0.170	1	0.78	0.160
470	0.181	1	0.93	0.003	500	0.238	1	0.63	0.164
470	0.203	1	1.05	0.004	500	0.300	1	0.46	0.143
470	0.270	1	0.92	0.057	500	0.364	1	0.10	0.047
470	0.339	1	0.86	0.068	500	0.490	1	0.00	0.000
470	0.409	1	0.88	0.085	500	0.614	1	0.00	0.000
470	0.452	2	0.84	0.107	500	0.748	1	0.00	0.000

[a] t = residence time (s). [b] Cell position 1 = 17.8 cm, 2 = 45.7 cm, and 3 = 81.2 cm. [c] $[CH_3OH]_0$ is the initial methanol concentration.

stream has a shorter residence time in the preheating section and subsequently has less time to complete decomposition prior to being mixed with fuel. Although the data have scatter, comparison of any pair of points with similar residence times and different optical module positions shows that the points having high flow rates produce similar reaction rates to those having low flow rates. If there were an appreciable population of H_2O_2 left after the shortest preheater residence time, there would be a significant difference in the observed oxidation rate. However, no such difference is observed, providing additional evidence that all of the H_2O_2 is converted to O_2 prior to mixing.

Figure 4 shows the results of oxidation for selected temperatures at an equivalence ratio of 0.85. The form of the data suggests a period of time before the bulk of the methanol reacts that also varies with temperature. In relating the analysis of the data to an elementary model, these two characteristic stages of the methanol consumption profile can be examined for their temperature dependence and then compared to Arrhenius factors of key steps in the mechanism identified by a sensitivity analysis. At 500 °C, the reaction is sufficiently fast that the 0.17 s minimum experimental time is not fast enough to measure the induction period with certainty. However, extrapolation of the 460−490 °C curves shows an induction time of approximately 0.2−0.6 s, corresponding to approximately the first 10% of conversion. During this period, the slope of the fuel

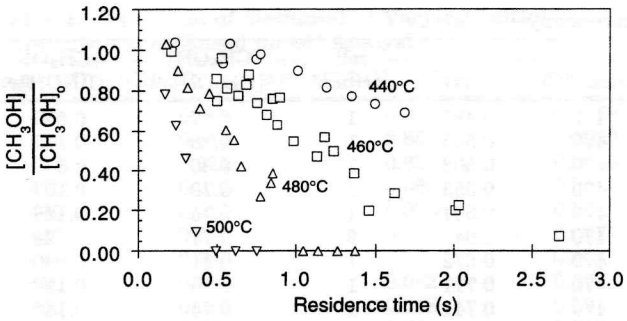

Figure 4. Measured normalized methanol concentration plotted versus residence time for an initial equivalence ratio of 0.85. Here, normalized refers to simply dividing the measured concentration of methanol by the known concentration in the feed. Results are shown for four of the seven isothermal conditions tested: 440 °C ○, 460 °C □, 480 °C △, and 500 °C ▽.

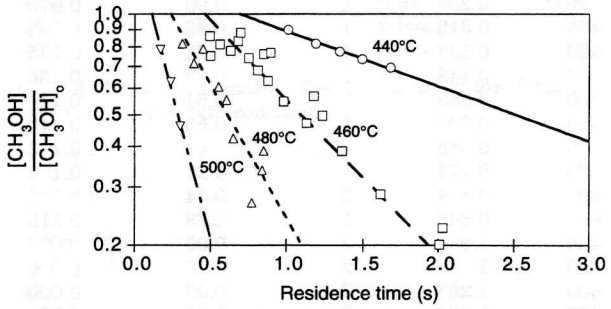

Figure 5. Plot of the same data in Figure 4 with normalized methanol concentrations >0.9 removed. The lines represent fits of the experimental data to $[CH_3OH]/[CH_3OH]_0 = \exp(-k_{eff}(t - t_{ind}))$ 440 °C ○—, 460 °C □– –, 480 °C △---, and 500 °C ▽—-.

Table 3. Parameters from the Induction Time Estimate

T (°C)	t_{ind} (s)	k_{eff} (s^{-1})	T (°C)	t_{ind} (s)	k_{eff} (s^{-1})
440	0.69	0.38	480	0.24	1.86
450	0.55	0.52	490	0.20	2.71
460	0.46	1.09	500	0.13	4.05
470	0.42	1.63			

disappearance curve is much less than during the final 90% of conversion.

In Figure 5 the data are replotted for normalized fuel concentrations <0.9. Assuming that the oxidation proceeds as first-order with respect to fuel, it is possible to linearly extrapolate back to $[CH_3OH]/[CH_3OH]_0 = 1.0$ and determine the apparent induction time, t_{ind}. Table 3 displays the results of the fit for

$$\frac{[CH_3OH]}{[CH_3OH]_0} = \exp(-k_{eff}(t - t_{ind})) \qquad (3)$$

Fitting the data to the expression in eq 3 produces two parameters. The first is the slope of a line that fits the data to exponential decay, with an offset in time. Physically, this can be interpreted as a bulk consumption rate constant, k_{eff}. The second is the intercept of this curve and the $[CH_3OH]/[CH_3OH]_0 = 1$ value on the ordinate. This is phenomenologically interpreted as a period of time during which little fuel is consumed prior to the bulk reaction. As this is a chemical system, and there are one or more chemical reactions taking place during this time, it is reasonable to expect that it would be an activated process and have Arrhenius behavior. It is apparent from Figure 5 that the data are well approximated by this description. Prior to the first-order regime, when most of the fuel is consumed, an induction period can be identified during which significantly slower methanol destruction rates are observed. This induction period can be assigned a characteristic rate constant by taking the reciprocal of the induction time, $(t_{ind})^{-1}$. Figure 6 shows an Arrhenius plot of both k_{eff} and $(t_{ind})^{-1}$. The slope of these two curves can be used to determine apparent activation energies for both time periods. The apparent activation energy for the bulk rate constant, k_{eff}, is 179 kJ/mol and for the induction rate constant, $(t_{ind})^{-1}$, is 118 kJ/mol.

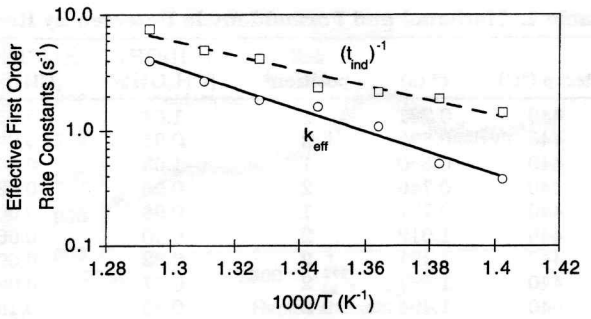

Figure 6. Arrhenius plot of the effective first-order rate constant, k_{eff}, and the inverse of the induction time, $(t_{ind})^{-1}$, versus $1000/T$. The lines represent least-squares fits to the experimental data: k_{eff} ○— and $(t_{ind})^{-1}$ □---.

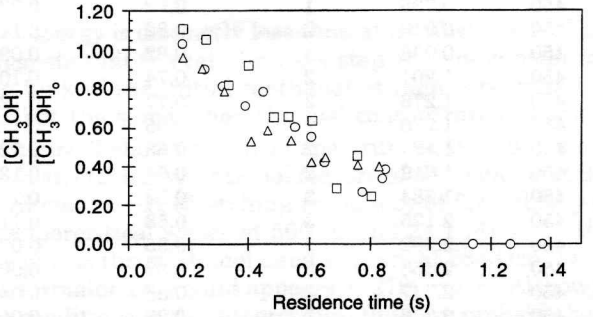

Figure 7. Measured normalized methanol concentration plotted versus residence time for three different initial equivalence ratios: 0.85 ○, 1.70 □, and 3.40 △.

Figure 7 shows a plot of the oxidation of methanol at three different reaction stoichiometries at 480 °C. Results for the other temperatures are similar, within the data scatter. The measurements indicate that the initial feed concentration of oxygen is not important in determining the reaction rate and that all three equivalence ratios react at the same rate until O_2 is exhausted. Thus, the use of the effective first-order rate to characterize the temperature dependence of the reaction over a wide concentration range, as is done is Figure 2, is not affected by the evolution of the oxygen stoichiometry as the reaction progresses.

Note that the methanol loss for the richest mixture corresponds to greater than stoichiometric oxygen consumption. For this case, there is only enough oxygen to convert 41% of the original methanol to CO_2; however, 60% was of the methanol was lost. This indicates that most of the methanol is effectively converted to formaldehyde and CO in rich conditions before CO_2 is produced.

The formaldehyde concentration has been measured using Raman spectroscopy, and the results are reported in Table 2. A selection of these data are plotted in Figure 8. Note that formaldehyde concentrations approach 19% of the initial methanol feed. After the accumulation of formaldehyde, it appears to be oxidized at a rate comparable to that of methanol. At 500 °C, only the decay of the formaldehyde is observed. For 490–450 °C both the accumulation and subsequent loss

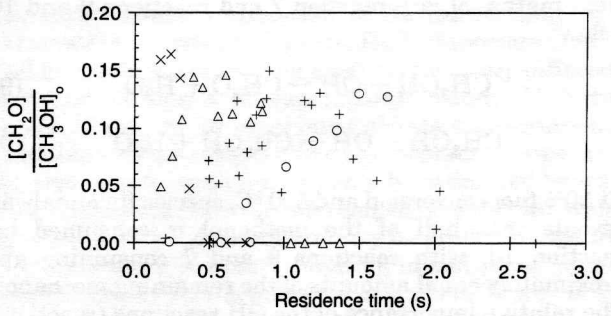

Figure 8. Measured normalized formaldehyde concentration plotted versus residence time for an initial equivalence ratio of 0.85. Results are shown for four of the seven isothermal conditions tested: 440 °C ○, 460 °C +, 480 °C △, and 500 °C ×.

are observed. At 440 °C measurements were not performed at sufficiently long residence times to observe the consumption of formaldehyde. Examining the production and destruction of formaldehyde provides important additional information to help determine the validity of detailed kinetic models, as discussed in the next section.

Before discussing the comparison of the experiments to elementary models, it is appropriate to comment on the likelihood of the reactor dimensions affecting the experimental results. Specifically, the role of the reactor walls in the oxidation process needs to be considered. Holgate and Tester (1994a) addressed this problem for H_2 and CO oxidation. Based on an experimental approach using a packed reactor, they determined that the walls did not significantly affect their results. However, flow reactors are routinely used in combustion research, and it has been demonstrated that they can be designed such that walls will not affect the results. Below we compare our system to typical combustion-conditions flow reactors.

From experimental conditions, collision rates may be calculated for walls and other reactant molecules from kinetic theory. The frequency of collisions experienced by an individual molecule per unit volume in an ideal gas is given by

$$Z_A = \sigma \bar{u} \rho^2 / (2)^{1/2} \tag{4}$$

and the frequency of wall collisions per unit area is given by

$$Z_W = \bar{u} \rho / 4 \tag{5}$$

where Z is the collision frequency, $\bar{u}$ is the mean molecular velocity, ρ is the molecular density, and σ is the molecular cross section (Moore, 1972). Taking the ratio of Z_W/Z_A and multiplying by the surface area to volume ratio of the reactor ($4/d$ for a tube, where d is the diameter) gives the fraction of collisions a molecule experiences, η, with a wall relative to those experienced with other species,

$$\eta = (2)^{1/2} / (\rho \sigma d) \tag{6}$$

Evaluating eq 6 for typical current experimental conditions, $\rho = 5$ mol/L or 3×10^{21} cm^{-3}, $d = 0.48$ cm, and $\sigma = 6.5 \times 10^{-16}$ cm^2 for water, yields $\eta = 1.5 \times 10^{-6}$. This indicates that a molecule has over 10^5 collisions within the fluid per wall collision. To compare this to other ambient-pressure, high-temperature flow reactors, note that the ratio is inversely proportional to d and ρ. For typical experimental conditions employed in a past atmospheric pressure study of CO and H_2 oxidation, i.e., $d = 10.32$ cm and temperature ≈ 1000 K (Yetter *et al.*, 1991), using $\sigma = 7.7 \times 10^{-16}$ cm^2 (for N_2) and $\rho = 0.012$ mol/L or 7.3×10^{18} cm^{-3} (for an ideal gas) gives $\eta = 2.4 \times 10^{-5}$. This corresponds to an equivalent reactor diameter for our conditions of 0.03 cm. Since this is over an order of magnitude smaller than our reactor diameter, we can conclude that wall reactions have minimal impact on our experimental results.

Comparison to Elementary Models. The measurements presented above provide the basis for interpreting the validity of existing elementary reaction schemes. Webley and Tester (1991) developed an elementary reaction model to predict the oxidation of methane and methanol in supercritical water. Their approach was to modify a successful kinetic scheme generated for high-temperature, gas phase oxidation. The model they used was the elementary scheme of Warnatz (1984) that successfully represented experiments in the 1000−2000 K range at ambient pressure. They made several key modifications to account for high density effects on unimolecular reaction rates and found that this mechanism successfully reproduced their methanol results. A particularly important modification was to express the unimolecular thermal decomposition rate of H_2O_2 in its high-pressure form, as suggested by the RRKM calculation given by Tsang and Hampson (1986).

Two related elementary mechanistic schemes which will be called Model 1 (Schmitt *et al.*, 1991) and Model 2 (Alkam *et al.*, 1995) have been developed more recently. These models were examined at constant temperature and pressure conditions using the computational package CHEMKIN Real Gas (Schmitt *et al.*, 1993), a modification of the CHEMKIN II (Kee and Miller, 1986) kinetics package, that accounts for nonidealities in the equations of state and employs a fugacity correction to the calculation of species thermodynamics and implicit reverse reaction rates. Model 1 was assembled from the H_2/O_2 mechanism of Miller and Bowman (1989), the methanol mechanisms of Norton and Dryer (1989, 1990) and Tsang (Tsang, 1987; Tsang and Hampson, 1986), and the C_2 reactions of Wilk *et al.* (1989, 1990) and Kaiser *et al.* (1986). The C_2 submechanism was omitted in our calculations after it was shown that these reactions had no impact on the methanol results. Model 2 was developed from Model 1 and successfully reproduced the results for CO and H_2 oxidation reported by Holgate and Tester (1994a) and also reproduces the methanol results reported by Tester *et al.* (1993).

There are two key distinctions between Model 1 and Model 2. First, Model 2 contains a modification to the forward rate of the reaction

$$CH_3OH + HO_2 \rightarrow CH_2OH + H_2O_2 \tag{7}$$

based on a correlation to similar reactions. This results in a rate constant 26 times slower than that calculated from the parameters given by Norton and Dryer (1989, 1990). The other major difference between Models 1 and 2 concerns the rate for the dissociation of hydrogen peroxide. The rate in Model 1 is 3.32 times greater at 500 °C than that in Model 2. This is a result of an attempt in Model 2 to use similar parameters to those for the H_2 and CO submechanism previously presented (Holgate and Tester, 1994b). It was found that these changes allowed Model 2 to reproduce more accurately the methanol experimental results of Tester *et al.* (1993). The cumulative effect of the two modifications

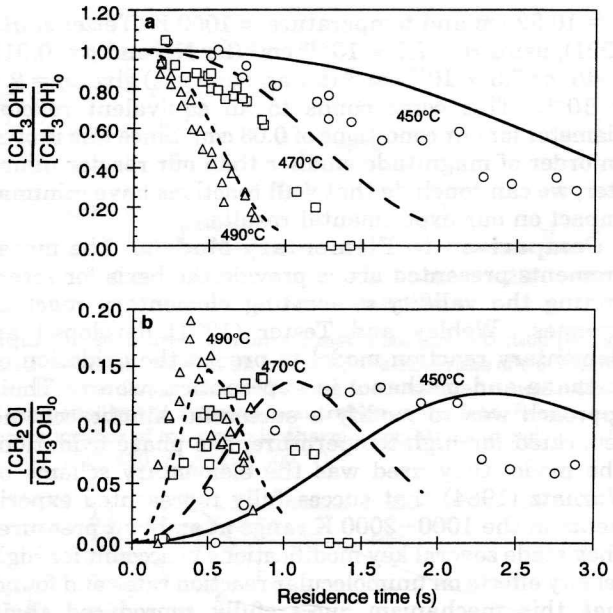

Figure 9. Comparison of experimental results (open symbols) to predictions from Model 1 (lines) for (a) methanol and (b) formaldehyde. Results are shown for three of the seven isothermal conditions tested: 450 °C ○—, 470 °C □– –, and 490 °C △---.

in Model 2 was to reduce the oxidation rate of methanol. The fuel consumption curves predicted by Model 2 have a much longer induction time as well as a longer bulk reaction time.

We find that Model 1 reproduces the current experimental results well, while Model 2 predicts rates nearly a factor of 10 too slow. Figure 9 presents a comparison of Model 1 and the experimental data for both methanol and formaldehyde at several of the experimental temperatures. The model predicts methanol oxidation rates to be slightly slower than observed experimentally. However, it predicts reasonably well the concentration of formaldehyde as well as the increase in peak concentration as temperature is raised. Note, however, that the model underpredicts the magnitude of this increase. For example, at 450 and 490 °C the model predicts a peak fraction of 0.13 and 0.15, respectively; however, the experiment reveals a change from 0.13 to approximately 0.19. The time difference observed for the predicted peak concentrations is a direct result of the slightly slower methanol oxidation rate predicted by the model.

Despite small differences between the model predictions and experimental results, Model 1 reproduces the data sufficiently well to use it for further analysis of the methanol oxidation process. Using both sensitivity and flux analysis techniques, key reactions have been identified that are crucial to reproducing the experimental results.

Methanol sensitivity analysis reveals that, after the induction period, the rate of the oxidation of methanol is most sensitive to the rate of the unimolecular dissociation of hydrogen peroxide:

$$H_2O_2 \rightleftarrows OH + OH \qquad (8)$$

This is not to be confused with residual hydrogen peroxide from the oxidizer line. As shown above, there is no H_2O_2 in this line when initially mixed with the fuel. This H_2O_2 is formed as an intermediate generated by the reacting system. Three other rate-controlling reactions, each of which involves hydrogen abstraction from methanol, are reaction 7 and reactions 9 and 10 below:

$$CH_3OH + OH \rightarrow CH_3O + H_2O \qquad (9)$$

$$CH_3OH + OH \rightarrow CH_2OH + H_2O \qquad (10)$$

At 50% fuel conversion and 500 °C, species flux analysis reveals that half of the methanol is consumed by reaction 10, with reactions 9 and 7 consuming approximately equal amounts of the remaining methanol. The relative importance of the OH reactions (reactions 9 and 10) increases significantly as the temperature is increased above 500 °C.

The induction period can also be characterized. Flux analysis reveals that first an initial O_2 must react with a methanol molecule to produce HO_2 and a reactive fuel radical. This is sufficient to initiate the chain branching steps on a time scale of 10^{-4} s. After this time, O_2 plays no significant role reacting with methanol and as a result, in agreement with Figure 7, does not affect the rate of methanol oxidation over a wide range of stoichiometries. The fuel radicals produced rapidly produce HO_2 and CH_2O by reaction with O_2. HO_2, in turn, reacts with fuel to produce H_2O_2 by reaction 7. The net effect of this cycle is to convert fuel to formaldehyde, O_2 to H_2O_2, and to preserve the chain propagating species HO_2. The rate of fuel consumption during the induction period is determined by the rate of the chain propagating step, reaction 7. The end of the induction period occurs when the concentration of H_2O_2 reaches a level where reaction 8 can supply the system with sufficient OH that reactions 9 and 10 consume most of the methanol. Flux analysis at 500 °C indicates that the combination of reactions 9 and 10 overtakes reaction 7 at approximately 0.11 s, in good agreement with the value of 0.13 s listed for the induction time in Table 3. The activation energies for reactions 7 and 8 in Model 1 are 79 and 209 kJ/mol, respectively. The observed activation energies for $(t_{eff})^{-1}$ and k_{eff} are 117 and 176, showing a trend consistent with Model 1.

The structure of this model breaks down at approximately 550 °C. This is the point in Figure 6 where the two curves would cross if extended. Above this temperature, there is no accumulation of H_2O_2, and OH oxidation chemistry dominates at all times. In the case of methanol this marks the distinction between low-temperature reactivity and the high-temperature combustion regime.

The peak formaldehyde concentration is controlled by the relative reaction rates of OH and HO_2 with methanol and formaldehyde. Methanol is oxidized by these radicals to form CH_3O and CH_2OH, both of which rapidly react to produce formaldehyde. Formaldehyde, in turn, is oxidized primarily by OH and HO_2 through hydrogen abstraction to form HCO, which subsequently reacts with O_2 to form CO. Quantitative examination of the amount of formaldehyde that accumulates tests a different part of the overall mechanism than does the examination of the loss of methanol. It confirms that the relative rates of attack by the oxidizing radicals, namely, OH and HO_2, on methanol and formaldehyde are approximately correct for Model 1. In contrast, in Model 2, at 490 °C, the formaldehyde fraction only reaches a maximum value of 0.07, much less than the measured 0.19, supporting the conclusion that the reaction rate for reaction 7 is incorrect in Model 2.

As a result of the importance of the dissociation of H_2O_2 in supercritical water for the oxidation of metha-

nol, independent verification of its dissociation rate parameters is critical. In fact, H_2O_2 dissociation may well be the rate-controlling reaction for many different oxidation processes in supercritical water. Unfortunately, there are no experimental rate measurements available for this temperature and pressure range, and the pressure dependence can only be estimated by way of RRKM calculations. In addition, on a molecular scale, the nature of this dissociation may be explicitly affected by the presence of water, resulting in additional buffer concentration dependencies not calculable by way of an RRKM method. Therefore, further investigation of this dissociation is crucial to future modeling efforts of hydrothermal water oxidation.

Conclusions

The oxidation of methanol has been measured in the temperature range from 440 to 500 °C, and the production of formaldehyde as a key intermediate has been determined. Experiments varying initial feed concentrations over 2 orders of magnitude indicate that higher initial methanol concentrations exhibit greater effective first-order rate constants than low feed concentrations. Using Raman spectroscopy, measurements of the absolute concentrations of methanol and formaldehyde were obtained in supercritical water. The experimental results reveal a brief induction period followed by first-order oxidation of the fuel. Predictions using several existing elementary reaction models were compared to the observed fuel consumption rates and the production and destruction rates of formaldehyde. Flux and sensitivity analysis techniques were used to identify key elementary reactions that need further examination at these reaction conditions. We have identified that the dissociation of hydrogen peroxide is not well characterized quantitatively but appears to be rate controlling during much of the reaction.

Acknowledgment

This work was supported by the DoD/DOE/EPA Strategic Environmental Research and Development Program (SERDP). One of us (Å.C.R.) was sponsored at Sandia by the Sweden–America Foundation, The Foundation BLANCEFLOR Boncompagni–Luduvisi née Bildt, OKs Miljöstiftelse, and Stiftelsen Bengt Lundqvists Minne. We thank W. J. Pitz (LLNL) and P. B. Butler (University of Iowa) for many useful discussions and for providing the details of their models in advance. We also thank R. R. Steeper, J. D. Aiken, and C. M. Griffith (Princeton University) for technical assistance.

Literature Cited

Abdullah, A. H.; Sherman, W. F. Variable Temperature High-Pressure Raman Cell. *J. Phys. E: Sci. Instrum.* **1980**, *13*, 1155–1159.

Alkam, M. K.; Pai, V. M.; Butler, P. B.; Pitz, W. J. Methanol and Hydrogen Oxidation Kinetics in Water at Supercritical States. *Combustion and Flame* **1995**, in press.

Armellini, F. J.; Tester, J. W. Experimental Methods for Studying Salt Nucleation and Growth from Supercritical Water. *J. Supercrit. Fluids.* **1991**, *4*, 254–264.

Armellini, F. J.; Tester, J. W. Solubility of Sodium Chloride and Sulfate in sub- and Supercritical Water Vapor from 450–550 °C and 100–250 bar. *Fluid Phase Equilib.* **1993**, *84*, 123–142.

Barner, H. E.; Huang, C. Y.; Johnson, T.; Martch, M. A.; Killilea, W. R. Supercritical Water Oxidation: An Emerging Technology. *J. Hazard. Mater.* **1992**, *31*, 1–17.

Eckbreth, A. C. *Laser Diagnostics for Combustion Temperature and Species*; Abacus Press: Cambridge, MA, 1988; Vol. 7.

Gloyna, E. F.; Li, L.; McBrayer, R. N. Engineering Aspects of Supercritical Water Oxidation. *Water Sci. Technol.* **1994**, *30*, 1–10.

Grasselli, J. G.; Bulkin, B. J. *Analytical Raman Spectroscopy*; John Wiley & Sons, Inc.: New York, 1991; Vol. 114.

Haar, L.; Gallagher, J. S.; Kell, G. S. *NBS/NRC Steam Tables: Thermodynamic and Transport Properties and Computer Programs for Vapor and Liquid States of Water in SI Units*; Hemisphere Publishing Corp.: New York, 1984.

Hanush, R. G.; Rice, S. F.; Hunter, T. B.; Aiken, J. D. Operation and Performance of the Supercritical Fluids Reactor. Report No. SAND96–8203; Sandia National Laboratories, 1995.

Helling, R. K.; Tester, J. W. Oxidation Kinetics of Carbon Monoxide in Supercritical Water. *Energy Fuels* **1987**, *1*, 417–423.

Holgate, H. R.; Tester, J. W. Oxidation of Hydrogen and Carbon Monoxide in Sub- and Supercritical Water: Reaction Kinetics, Pathways, and Water-Density Effects. 1. Experimental Results. *J. Phys. Chem.* **1994a**, *98*, 800–809.

Holgate, H. R.; Tester, J. W. Oxidation of Hydrogen and Carbon Monoxide in Sub- and Supercritical Water: Reaction Kinetics, Pathways, and Water-Density Effects. 2. Elementary Reaction Modeling. *J. Phys. Chem.* **1994b**, *98*, 810–822.

Kaiser, E. W.; Westbrook, C. K.; Pitz, W. J. Acetaldehyde Oxidation in the Negative Temperature Coefficient Regime: Experimental and Modeling Results. *Int. J. Chem. Kinet.* **1986**, *18*, 655–688.

Kee, R. J.; Miller, J. A. *CHEMKIN-II: A Structured Approach to the Computational Modeling of Chemical Kinetics and Molecular Transport in Flowing Systems*, ver. 4.3, Combustion Chemistry Division, Sandia National Laboratories, Livermore, CA, 1986.

Li, L.; Chen, P.; Gloyna, E. F. Generalized Kinetic Model for Wet Oxidation of Organic Compounds. *AIChE J.* **1991**, *37*, 1687–1697.

Masten, D. A.; Foy, B. R.; Harradine, D. M.; Dyer, R. B. In Situ Raman Spectroscopy of Reactions in Supercritical Water. *J. Phys. Chem.* **1993**, *97* (33), 8557–8559.

McBrayer, R. N. Design and Operation of the First Commercial Supercritical Water Oxidation Facility. First International Workshop on Supercritical Water Oxidation, Jacksonville, FL, 1995, Session IV: SCWO Technology Development Demonstrations.

Miller, J. A.; Bowman, C. T. Mechanism and Modeling of Nitrogen Chemistry in Combustion. *Prog. Energy Combust. Sci.* **1989**, *15*, 287–338.

Modell, M. Processing Methods for the Oxidation of Organics in Supercritical Water.; U.S. Patent 4,543,190, 1985.

Moore, W. J. *Physical Chemistry*; Prentice-Hall: Englewood Cliffs, NJ, 1972.

Nestor, J. R.; Lippincott, E. R. The Effect of the Internal Field on Raman Scattering Cross Sections. *J. Raman Spectrosc.* **1973**, *1*, 305–318.

Norton, T. S.; Dryer, F. L. Some New Observations on Methanol Oxidation Chemistry. *Combust. Sci. Technol.* **1989**, *63*, 107–129.

Norton, T. S.; Dryer, F. L. Toward a Comprehensive Mechanism for Methanol Pyrolysis. *Int. J. Chem. Kinet.* **1990**, *22*, 219–241.

Sadtler. *The Sadtler Standard Raman Spectra*; Sadtler Research Laboratories, subsidiary of Block Engineering: Philadelphia, PA, 1973.

Schmitt, R. G.; Butler, P. B.; Bergan, N. E.; Pitz, W. J.; Westbrook, C. K. Destruction of Hazardous Waste in Supercritical Water. Part II: A Study of High-Pressure Methanol Oxidation Kinetics. 1991 Fall Meeting of the Western States Section/The Combustion Institute, University of California at Los Angeles, CA, 1991, 19.

Schmitt, R. G.; Butler, P. B.; French, N. B. CHEMKIN Real Gas: A FORTRAN Package for Analysis of Thermodynamic Properties and Chemical Kinetics in Nonideal Systems; University of Iowa, Report No. UIME PBB 93-006, 1993.

Shaw, R. W.; Brill, T. B.; Clifford, A. A.; Eckert, C. A.; Franck, E. U. Supercritical Water. *Chem. Eng. News* **1991**, *69*, 26–39.

Spohn, P. D.; Brill, T. B. Raman Spectra of the Species in Concentrated Aqueous Solutions of $Zn(NO_3)_2$, $Ca(NO_3)_2$, $Cd(NO_3)_2$, $LiNO_3$, and $NaNO_3$ up to 450 °C and 30 MPa *J. Phys. Chem.* **1989**, *93*, 6224.

Steeper, R. R. Methane and Methanol Oxidation in Supercritical Water: Chemical Kinetics and Hydrothermal Flame Studies, Report No. SAND96-8208, Sandia National Laboratories, 1995.

Steeper, R. R.; Rice, S. F.; Brown, M. S.; Johnston, S. C. Methane and Methanol Diffusion Flames in Supercritical Water. *J. Supercrit. Fluids* **1992**, *5* (4), 262–268.

Steeper, R. R.; Rice, S. F.; Kennedy, I. M.; Aiken, J. D. Kinetics Measurements of Methane Oxidation in Supercritical Water. *J. Phys. Chem.* **1996**, *100*, 184–189.

Surkin, R. I.; Sverdlov, L. M. Relative Raman Scattering Cross Sections of Some Gases and Vapors that Pollute the Atmosphere. *Opt. Spectrosc.* **1980**, *48* (2), 139–140.

Swallow, K. C.; Killilea, W. R.; Malinowski, K. C.; Staszak, C. N. The MODAR Process for the Destruction of Hazardous Organic Wastes-Field Test of a Pilot-Scale Unit. *Waste Manage.* **1989**, *9*, 19–26.

Takagi, J.; Ishigure, K. Thermal Decomposition of Hydrogen Peroxide and Its Effect on Reactor Water Monitoring of Boiling Water Reactors. *Nucl. Sci. Eng.* **1985**, *89*, 177–186.

Tester, J. W.; Holgate, H. R.; Armellini, F. J.; Webley, P. A.; Killilea, W. R.; Hong, G. T.; Barner, H. E. *Supercritical Water Oxidation Technology Process Development and Fundamental Research*; Tedder, D. W., Pohland, F. G., Eds.; Emerging Technologies in Hazardous Waste Management III; American Chemical Society: Washington, DC, 1991; pp 35–76.

Tester, J. W.; Webley, P. A.; Holgate, H. R. Revised Global Kinetic Measurements of Methanol Oxidation in Supercritical Water. *Ind. Eng. Chem. Res.* **1993**, *32*, 236–239.

Tsang, W. Chemical Kinetic Data Base for Combustion Chemistry. Part 2. Methanol. *J. Phys. Chem. Ref. Data* **1987**, *16*, 471–508.

Tsang, W.; Hampson, R. F. Chemical Kinetic Data Base for Combustion Chemistry. Part 1. Methane and Related Compounds. *J. Phys. Chem. Ref. Data* **1986**, *15*, 1087–1279.

Warnatz, J. Rate Coefficients in the C/H/O System, Chapter 5. In *Combustion Chemistry*; Gardiner, W. C., Jr., Ed.; Springer-Verlag: New York, 1984.

Webley, P. A.; Tester, J. W. *Fundamental Kinetics of Methanol Oxidation in Supercritical Water*; Johnston, K. P., Penninger, J. M. L., Eds.; Supercritical Fluid Science and Technology; American Chemical Society: Washington, DC, 1989; pp 259–275.

Webley, P. A.; Tester, J. W. Fundamental Kinetics of Methane Oxidation in Supercritical Water. *Energy Fuels* **1991**, *5*, 411–419.

Wilk, R. D.; Cernansky, N. P.; Pitz, W. H.; Westbrook, C. K. Propene Oxidation at Low and Intermediate Temperatures: A Detailed Kinetic Study. *Combust. Flame* **1989**, *77*, 145–170.

Wilk, R. D.; Pitz, W. J.; Westbrook, C. K.; Cernansky, N. P. Chemical Kinetic Modeling of Ethene Oxidation at Low and Intermediate Temperatures. Twenty-Third Symposium (International) on Combustion, Orleans, France, 1990, 203–210.

Yetter, R. A.; Dryer, F. L.; Rabitz, H. Flow Reactor Studies of Carbon Monoxide/Hydrogen/Oxygen Kinetics. *Combust. Sci. Technol.* **1991**, *79*, 129–140.

Received for review August 17, 1995
Accepted April 2, 1996[⊗]

IE950510F

[⊗] Abstract published in *Advance ACS Abstracts,* May 15, 1996.